Annals of Physics 387 (2017) 334–347

Contents lists available at ScienceDirect

Annals of Physics

journal homepage: www.elsevier.com/locate/aop

Experimental test of entangled histories

Jordan Cotler [a,*], Lu-Ming Duan [b,c], Pan-Yu Hou [b], Frank Wilczek [d,e], Da Xu [b,f], Zhang-Qi Yin [b], Chong Zu [b]

[a] Stanford Institute for Theoretical Physics, Department of Physics, Stanford University, USA
[b] Center for Quantum Information, Institute for Interdisciplinary Information Sciences, Tsinghua University, Beijing 100084, China
[c] Department of Physics, University of Michigan, Ann Arbor, MI 48109, USA
[d] Center for Theoretical Physics, MIT, Cambridge MA 02139, USA
[e] Origins Project, Arizona State University, Tempe AZ 25287, USA
[f] Department of Physics, Tsinghua University, Beijing 100084, China

ARTICLE INFO

Article history:
Received 4 October 2016
Accepted 11 September 2017
Available online 25 September 2017

Keywords:
Temporal entanglement
Many worlds
Consistent histories

ABSTRACT

Entangled histories arise when a system partially decoheres in such a way that its past cannot be described by a sequence of states, but rather a superposition of sequences of states. Such entangled histories have not been previously observed. We propose and demonstrate the first experimental scheme to create entangled history states of the Greenberger–Horne–Zeilinger (GHZ) type. In our experiment, the polarization states of a single photon at three different times are prepared as a GHZ entangled history state. We define a GHZ functional which attains a maximum value 1 on the ideal GHZ entangled history state and is bounded above by 1/16 for any three-time history state lacking tripartite entanglement. We have measured the GHZ functional on a state we have prepared experimentally, yielding a value of 0.656 ± 0.005, clearly demonstrating the contribution of entangled histories.

1. Introduction

The traditional "observables" of quantum theory are operators in Hilbert space that act at a particular time. But many quantities of physical interest, such as the accumulated phase

* Corresponding author.
E-mail addresses: jcotler@stanford.edu (J. Cotler), lmduan@umich.edu (L.-M. Duan), yinzhangqi@mail.tsinghua.edu.cn (Z.-Q. Yin).

https://doi.org/10.1016/j.aop.2017.09.004
0003-4916/

$\exp i \int_1^2 dt\, \vec{v} \cdot \vec{A}$ of a particle moving in an electromagnetic potential, its accumulated proper time, or some other sequence of specified properties, are more naturally expressed in terms of histories. Having performed a measurement of a more general, history-dependent sort of observable, we partially decohere the history of a system to a sequence or even a superposition of sequences of events, which lives in an eigenspace of a temporally extended Hilbert space.

Recently two of us, building on the work of Griffiths and others [1], have formulated a mathematical framework which extends many of the concepts and procedures ordinarily used in analyzing *states* of quantum systems to their *histories* [2–4]. While the formalism is equivalent to standard quantum mechanics, it elucidates the temporal structure of sequences of events, which is not transparent in more standard formulations in which one considers quantum states at fixed times. The formalism allows one to ask and answer questions about temporal structure which are not obvious in standard formulations, and provides a valuable tool for manipulating and calculating with temporal sequences of states.

Specifically, we have constructed, under very general assumptions about a quantum dynamical system, a Hilbert space of its possible histories. The inner product reflects probabilities of histories occurring. There is a natural definition of observables on the history Hilbert space. It accommodates the observables we mentioned initially, and new possibilities which might not have been easy to imagine otherwise. The result of measuring a history observable is a partial reconstruction of "what happened" during the evolution of one's system. Analogously to how measurement of the value of an ordinary observable on a system establishes the location of the state of the system within an eigenspace of the observable, measurement of a history observable on a system's evolution establishes the location of its history within an eigenspace (in history space) of the history observable. Such eigenspaces often contain *entangled* histories. The defining property of an entangled history is that it does not correspond to a definite sequence of states in time. In other words, there is a superposition of multiple timelines of sequences of events that describe the past.

A particularly interesting sort of entangled history corresponds to a particular state at an initial time, and to another particular state at a final time, and yet can not be assigned to a definite state at intermediate times since multiple *sequences* of states have occurred in superposition. Such an entangled history provides a vivid illustration of the "many worlds" picture of quantum mechanics, for it branches into several incompatible trajectories, which later come together. It is interesting to study entangled histories since they enable a concrete probe of the sort of partially decohered states which are integral to many worlds, and which provide us with our best description of the past. Indeed, entangled histories suggest that our description of the past after partial decoherence is more interesting than previously thought, and comprises of multiple interwoven timelines. Such entangled histories arise in nature when quantum records of *sequences* of past events become strongly entangled with the environment and then partially decohere.

Here we describe a detailed protocol for producing an entangled history of that kind. We have produced histories following that protocol, and measured that they display behavior which cannot be realized by any history which is not entangled. Our history state is a temporal analogue of the GHZ state, and our measurement strategy was inspired by the GHZ test. Hence it is appropriate briefly to describe the nature of that test, and its context.

In 1935, Einstein, Podolsky and Rosen (EPR) noted a peculiar consequence of quantum theory, according to which measurement outcomes of distant entangled particles should be perfectly correlated — a result they felt to be in tension with relativistic locality (which limits causal influence by the speed of light) [5]. In 1964, John Bell proved that the predictions of quantum theory differ quantitatively from any that can emerge from a large class of deterministic (classical) local models [6] (later, all local-causal models were shown to be ruled out as well [7]). Following Bell's suggestion, numerous experiments have been done, and confirmed quantum theory [8–10]. In 1989, Greenberger, Horne, and Zeilinger proposed a related test which is slightly more complicated to set up experimentally, but much simpler to interpret and more striking theoretically [11]. In particular, the GHZ test demonstrates non-classical correlations deterministically, as opposed to the statistically non-classical correlations captured by the Bell test. The GHZ test was made transparent by Mermin [12], brilliantly expounded by Coleman [13], and performed by Pan et al. [14]. The experiment we performed was in large part inspired by the work of Mermin and the exposition and commentary of Coleman.

A particular multipartite entangled state called the GHZ state, which involves at least three spin-1/2 degrees of freedom, is essential for the GHZ test. In our proposal, we deal with the properties of one photon at three different times, rather than three photons at the same time. Below, we define a functional $\mathcal{G}$ which is diagnostic of entangled histories. We will prove that for product history states $\mathcal{G}$ is bounded above by 0, while for history states lacking tripartite entanglement it is bounded above by 1/16. For ideal GHZ entangled histories, the functional $\mathcal{G}$ is equal to 1.

Motivated by these ideas, we performed the GHZ test for entangled histories experimentally. We generated a candidate GHZ entangled history state for a single photon, and measured its $\mathcal{G}$ functional. We measure $\mathcal{G}$ to be 0.656 ± 0.005, which considerably exceeds the bounds mentioned previously. Therefore, the GHZ test for histories clearly demonstrates the existence of entangled histories.

We should add that the structure of our temporal analogue of the GHZ test does not preclude its classical modeling in the sense that there is a classical experiment which reproduces the same measurement statistics. Indeed, in appropriate limits our setup can be understood on the basis of classical optics (which anticipates key features of quantum theory, i.e. complex waves which interfere, and whose absolute square is physically salient). However, our experiment works with individual photons which cannot be described by non-quantum theory. Still, it seems to us noteworthy that a simple stochastic classical model for the functional $\mathcal{G}$ has an upper bound of 1/16. (See Appendix.) While that classical model does not map onto our experiment cleanly, its analysis is instructive.

We should also mention that a very interesting, but quite distinct aspect of temporal correlation in quantum theory has been the subject of previous study [15–26]. These works, including the Leggett–Garg inequalities, focus on temporal correlations induced by the usual quantum measurement process, whereas we are primarily concerned with correlations that are intrinsic to an unmeasured system. More specifically, previous studies have analyzed how measurements of a system, no matter how non-invasive these measurements may be, introduce types of temporal correlations. These temporal correlations cannot be reproduced by classical theories in which measurement does not affect the state of a system. Indeed, measuring the state of a system projects it onto a particular basis in Hilbert space, which can both break correlations with the past and induce new correlations with future measurements in similar or different bases. By contrast, our setup restores a quantum state after measurement to its quantum state from before the measurement, so as not to introduce additional correlations by virtue of the measurement itself. We seek to understand correlations between a state and a unitarily evolved version of itself, which we can only access if we correct for the effect of intermediate measurements.

There has also been recent work on precise characterizations of certain types of temporal correlations in quantum systems, and their use as an information-theoretic resource [27–30]. These results are a temporal analog of more standard spatial quantum steering, and are of a different character than the results of the entangled histories framework.

To summarize, we are interested in temporal correlations intrinsic to histories which are *not* due to intermediate measurements. We show that the temporal correlations in our system cannot be reproduced by a single history, and hence our system produces an entangled history. These concepts will be elaborated below.

2. Constructing an entangled history state

In Griffith's theory of "Consistent Histories" [1] and its generalizations [2,31–39], a history state is a sum of tensor-like event products, in the form

$$|\Psi) = \hat{P}^{i_n}_{t_n} \odot \cdots \odot \hat{P}^{i_3}_{t_3} \odot \hat{P}^{i_2}_{t_2} \odot \hat{P}^{i_1}_{t_1} \tag{1}$$

Here the $P^{i_j}_{t_j}$ are projectors at different times in temporal order $t_1 < t_2 < t_3 < \cdots < t_n$ where the index i distinguishes orthogonal projectors within a decomposition of the identity. $\odot$ is a typographical variation on the tensor product symbol $\otimes$, which we use when the factors in tensor product refer to different times. An inner product on history space is defined by

$$(\Psi|\Phi) \;=\; \mathrm{Tr}(K^\dagger|\Psi)\,K|\Phi)) \tag{2}$$

where

$$K(|\Psi) = \hat{P}^{i_n}_{t_n} T(t_n, t_{n-1}) \cdots \hat{P}^{i_3}_{t_3} T(t_3, t_2) \hat{P}^{i_2}_{t_2} T(t_2, t_1) \hat{P}^{i_1}_{t_1} \tag{3}$$

Using this positive semi-definite inner product we can define quantum superposition and quantum interference for *histories* just as we do for quantum states. For a more detailed exposition, see [2].

Let us discuss, conceptually, how we might construct the GHZ history state

$$|\mathrm{GHZ}) := \frac{1}{\sqrt{2}} \left([z^+] \odot [z^+] \odot [z^+] - [z^-] \odot [z^-] \odot [z^-] \right), \tag{4}$$

where the notation $|\cdot)$ is used to denote the history state, and where $[z^\pm] := |z^\pm\rangle\langle z^\pm|$. The GHZ history state indicates that the past is described by a superposition of two *sequences* of events: namely, the particle's evolution was $|z^+\rangle \leftarrow |z^+\rangle \leftarrow |z^+\rangle$ *and* $|z^-\rangle \leftarrow |z^-\rangle \leftarrow |z^-\rangle$. We have written these sequences from right to left to match our notation for histories.

Consider a spin-1/2 particle in the state $|x^+\rangle = \frac{1}{\sqrt{2}}(|z^+\rangle + |z^-\rangle)$. We are going to construct an entangled history state via a post-selection procedure [18,40–44]. We introduce three auxiliary qubits $|0\rangle_1|0\rangle_2|0\rangle_3 =: |000\rangle$. At time t_1 we perform a CNOT operation between the first auxiliary qubit and the spin-1/2 particle, resulting in

$$\frac{1}{\sqrt{2}} |z^+\rangle|000\rangle + \frac{1}{\sqrt{2}} |z^-\rangle|100\rangle \tag{5}$$

We let this system evolve trivially to time t_2. Then at time t_2, we perform a CNOT between the second auxiliary qubit and the spin-1/2 particle, resulting in

$$\frac{1}{\sqrt{2}} |z^+\rangle|000\rangle + \frac{1}{\sqrt{2}} |z^-\rangle|110\rangle \tag{6}$$

The system then evolves trivially to time t_3, at which time we perform a CNOT between the third auxiliary qubit and the spin-1/2 particle, giving

$$\frac{1}{\sqrt{2}} |z^+\rangle|000\rangle + \frac{1}{\sqrt{2}} |z^-\rangle|111\rangle \tag{7}$$

If we measure the auxiliary qubits in the $\{|000\rangle, |111\rangle, \ldots\}$ basis, then measuring $|000\rangle$ would indicate that the spin-1/2 particle has been in the history state $[z^+]\odot[z^+]\odot[z^+]$; and if we measure $|111\rangle$, this would indicate that the spin-1/2 particle has been in the history state $[z^-]\odot[z^-]\odot[z^-]$. However we can also choose to measure the auxiliary qubits in the GHZ basis $\left\{ \frac{1}{\sqrt{2}}(|000\rangle \pm |111\rangle), \ldots \right\}$. Then if we measure $\frac{1}{\sqrt{2}}(|000\rangle - |111\rangle)$, it means that the spin-1/2 particle has been in the history state $[z^+]\odot[z^+]\odot[z^+]$ with amplitude $1/\sqrt{2}$, *and* $[z^-]\odot[z^-]\odot[z^-]$ with amplitude $-1/\sqrt{2}$. In other words, the particle has been in the entangled history state $\frac{1}{\sqrt{2}} \left([z^+] \odot [z^+] \odot [z^+] - [z^-] \odot [z^-] \odot [z^-] \right)$. By changing the basis of the auxiliary qubits, we have *erased* knowledge about the history of the spin-1/2 particle. As emphasized in [45], selective erasure can be a powerful tool for exploring quantum interference phenomena.

Similar techniques have been proposed in the context of "multiple-time states" [40]. In this language, we can write the temporal GHZ state as $\frac{1}{\sqrt{2}} \left(\langle z^+|\,|z^+\rangle\langle z^+|\,|z^+\rangle\langle z^+|\,|z^+\rangle - \langle z^-|\,|z^-\rangle\langle z^-|\,|z^-\rangle\langle z^-|\,|z^-\rangle \right)$. The interpretation of temporal entanglement has been a subject of much debate [40,46,47]. The framework proposed in [2–4], grounded in the consistent histories approach of Griffiths [1], seems to us clear and unambiguous.

3. Temporal GHZ test

In this section we will discuss how to perform a GHZ test for entangled histories. Consider the operators

$$\sigma_x \odot \sigma_y \odot \sigma_y \,, \qquad \sigma_y \odot \sigma_x \odot \sigma_y \,, \qquad \sigma_y \odot \sigma_y \odot \sigma_x \,, \qquad \sigma_x \odot \sigma_x \odot \sigma_x \tag{8}$$

on a three-time history space of a single spin-1/2 particle with trivial time evolution. The expectation values of $|\mathrm{GHZ}\rangle$ with the history state operators corresponding to the four operators in Eq. (8) are 1, 1, 1 and -1, respectively. The product of these four expectation values is -1. We represent this procedure of computing the product of the expectation values by the functional $\mathcal{G}$ which satisfies

$$\mathcal{G}[|\Psi\rangle] = -\langle\sigma_x \odot \sigma_x \odot \sigma_x\rangle\langle\sigma_y \odot \sigma_y \odot \sigma_x\rangle\langle\sigma_y \odot \sigma_x \odot \sigma_y\rangle\langle\sigma_x \odot \sigma_y \odot \sigma_y\rangle \tag{9}$$

where $|\Psi\rangle$ is a normalized history state. For the ideal GHZ history state, we have

$$\mathcal{G}[|\mathrm{GHZ}\rangle] = 1 \tag{10}$$

We can write a history state with two-time entanglement as $|\psi\rangle \odot \begin{bmatrix} \cos^2(\theta) & \cos(\theta)\sin(\theta)\, e^{-i\phi} \\ \cos(\theta)\sin(\theta)\, e^{i\phi} & \sin^2(\theta) \end{bmatrix}$, where $|\psi\rangle$ is arbitrary two-time entangled history states. Other history states with two-time entanglement take the same form, up to permutations of the tensor product components. Since the $\mathcal{G}$ functional is not sensitive to such permutations, it suffices to consider a single ordering. We have proved that (Appendix)

$$\mathcal{G}\left(|\psi\rangle \odot \begin{bmatrix} \cos^2(\theta) & \cos(\theta)\sin(\theta)\, e^{-i\phi} \\ \cos(\theta)\sin(\theta)\, e^{i\phi} & \sin^2(\theta) \end{bmatrix}\right) = -\frac{1}{4}\sin^4(2\theta)\sin^2(2\phi)\langle\sigma_x \odot \sigma_x\rangle\langle\sigma_y \odot \sigma_y\rangle\langle\sigma_x \odot \sigma_y\rangle\langle\sigma_y \odot \sigma_x\rangle \leq \frac{1}{16} \tag{11}$$

And for a generic separable history state

$$|\psi_{\mathrm{pure}}\rangle \equiv P(\theta_1, \phi_1) \odot P(\theta_2, \phi_2) \odot P(\theta_3, \phi_3) \tag{12}$$

where $P(\theta, \phi) = \begin{bmatrix} \cos^2(\theta) & \cos(\theta)\sin(\theta)\, e^{-i\phi} \\ \cos(\theta)\sin(\theta)\, e^{i\phi} & \sin^2(\theta) \end{bmatrix}$, we have

$$\mathcal{G}[|\psi_{\mathrm{pure}}\rangle] = -\frac{1}{64}\sin^4(2\theta_1)\sin^4(2\theta_2)\sin^4(2\theta_3)\sin^2(2\phi_1)\sin^2(2\phi_2)\sin^2(2\phi_3) \leq 0 \tag{13}$$

Our goal is to construct an approximation to the history state $|\mathrm{GHZ}\rangle$ experimentally, and to show that for our constructed state $\mathcal{G}[|\mathrm{GHZ}\rangle] \gg 1/16$, thus demonstrating a high degree of temporal entanglement. (In fact the $\mathcal{G}$ functional even distinguishes a specific form of tripartite entanglement. For the W entangled history state, $|W\rangle = \frac{1}{\sqrt{3}}\left([z^-] \odot [z^+] \odot [z^+] + [z^+] \odot [z^-] \odot [z^+] + [z^+] \odot [z^+] \odot [z^-]\right)$, the $\mathcal{G}$ functional vanishes.) This τGHZ test (i.e., temporal GHZ test) is much simpler than the generalized temporal Bell test in [3], and requires many fewer measurements.

4. Experimental results

We have phrased our discussion in the language appropriate to the spin states of a spin-$\frac{1}{2}$ particle. As is well known, we can use the same two-dimensional, complex state space to describe the polarization states of a photon. In that context, it is known as the Poincaré sphere. We can adapt standard optical tools and techniques to create a temporal GHZ state for a photon and measure the correlations that appear in the GHZ functional. The predicted correlations, as we have seen, provide quantitative evidence for the contribution of highly entangled histories.

Before proceeding, we provide a "dictionary" between the complex state space of a spin-1/2 particle and the polarization state of a single photon. We make the identifications

$$\begin{aligned} |z^+\rangle &\longleftrightarrow |H\rangle \\ |z^-\rangle &\longleftrightarrow |V\rangle \\ |x^+\rangle &\longleftrightarrow |D\rangle \\ |x^-\rangle &\longleftrightarrow |A\rangle \\ |y^+\rangle &\longleftrightarrow |R\rangle \\ |y^-\rangle &\longleftrightarrow |L\rangle \end{aligned}$$

where "H" stands for "horizontally" polarized light, "V" stands for "vertically" polarized light, "D" stands for "diagonally" polarized light, "A" stands for "anti-diagonally" polarized light, "R" stands for "right-circularly" polarized light, and "L" stands for "left-circularly" polarized light. We have the standard relations

$$|D\rangle = \frac{1}{\sqrt{2}}\left(|H\rangle + |V\rangle\right) \tag{14}$$

$$|A\rangle = \frac{1}{\sqrt{2}}\left(|H\rangle - |V\rangle\right) \tag{15}$$

$$|R\rangle = \frac{1}{\sqrt{2}}\left(|H\rangle + i|V\rangle\right) \tag{16}$$

$$|L\rangle = \frac{1}{\sqrt{2}}\left(|H\rangle - i|V\rangle\right) \tag{17}$$

To implement the GHZ test for entangled histories experimentally, we prepare a single photon through spontaneous parametric down conversion (SPDC) shown in Fig. 1. The SPDC process generates photon pairs with perpendicular polarizations, which are then separated by a polarizing beamsplitter (PBS). Through detection of the reflected photon by an avalanche photodiode single photon detector (D1), we get a single photon source on the other outport (Fiber coupler 3). We prepare this (approximate) single photon as a diagonal polarization state $[D]$ with a fiber-based polarization controller (PC) and a polarizer, and then send it into a balanced Mach–Zehnder interferometer (MZI), each arm of which supports a sequence of PBSs and wave-plate sets (WP). The incoming photon in the $[D]$ state is initially split, by PBS0, into horizontal (H) and vertical (V) components of equal amplitude, traveling along the two arms. WP2 and PBS2 divide the photon in the lower arm again, removing one polarization direction, while the other continues along the arm. We might, for example, remove the $[L]$ polarization, while allowing $[R]$ to continue propagating. WP4 then rotates the propagating photon back to $[H]$ direction. Two more operations (PBS4, WP6 and PBS6, WP8) of the same type take place, until the surviving photon reaches PBS7. The surviving photon will have been in the history state $[H] \odot [H] \odot [H]$, and sampled by the observable $[R] \odot * \odot *$, where the wild cards reflect our choices of polarization for PBS4 and PBS6. A completely parallel analysis applies to the other arm. Finally, the surviving components recombine coherently at PBS7, another polarizing beam splitter, and emerge in a direction that enforces a relative minus sign between the contributions from $[H] \odot [H] \odot [H]$ and $[V] \odot [V] \odot [V]$. By post-selecting on the events that trigger D2, and varying the wave-plate sets appropriately, we can measure the GHZ functional for an entangled history. We must measure the expectation values $\langle \sigma_x \odot \sigma_x \odot \sigma_x \rangle$, $\langle \sigma_y \odot \sigma_y \odot \sigma_x \rangle$, $\langle \sigma_y \odot \sigma_x \odot \sigma_y \rangle$ and $\langle \sigma_x \odot \sigma_y \odot \sigma_y \rangle$ with respect to the GHZ history state, and then multiply all of the expectation values together (see the detailed experimental design in the Appendix for the encoding of 3 auxiliary qubits into the path degree of freedom of a single photon). Note that our experiment is implemented by a sequence of projective measurements and post-selection instead of non-demolition ancilla-assisted measurements as was discussed earlier. However, our chosen methodology does not affect the outcome of the experiment or interpretation as entangled histories, and is easier to implement.

In this experiment we often access polarization properties at definite times, through PBS1 − 6. Alternatively, in the case where the photon transmits at all of the 6 PBSs and triggers D2, we access a multi-time observable. Such multi-time observables represent, in Griffiths' terminology [1], "contextual" properties. We can form a family based on those complementary single-time and multi-time properties. The character of the history state $\frac{1}{\sqrt{2}}([z^+] \odot [z^+] \odot [z^+] - [z^-] \odot [z^-] \odot [z^-])$ emerges clearly only when we measure multi-time observables, which we in turn access when certain other events fail to occur.

The experimental procedure is divided into 32 trials, which each have separate settings for the polarizing beam splitters and wave-plates. Each trial consists of preparing the settings of the apparatus and recording the number of photons received by detector D2 (denoted by Counts(D2)). We define

$$x_1 = D\,, \qquad x_2 = A\,, \qquad x_3 = R\,, \qquad x_4 = L$$
$$\bar{x}_1 = A\,, \qquad \bar{x}_2 = D\,, \qquad \bar{x}_3 = L\,, \qquad \bar{x}_4 = R$$

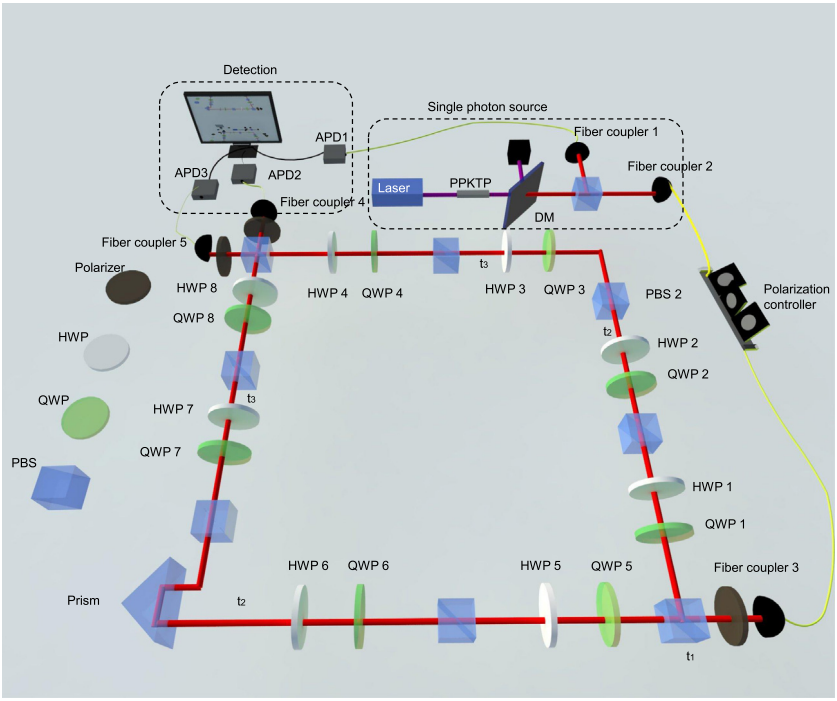

Fig. 1. Illustration of the experimental setup. A continuous-wave diode laser around 404 nm in wavelength, after a band-pass filter centered at 404 nm with 3 nm bandwidth, is focused on a type II PPKTP crystal to generate correlated photon pairs of 808 nm wavelength with perpendicular polarizations through spontaneous parametric down conversion. A dichroic mirror (DM) is used to filter out the pump beam. The photon pairs are split by a polarizing beam splitter (PBS), and then coupled into single mode fibers. With the registration of a photon count at a fiber-based single photon detector D1, we get a heralded single photon source in the other fiber outport (fiber coupler 3). The polarization of the heralded photon is set to the state $|D\rangle = (|H\rangle + |V\rangle)/\sqrt{2}$ with a fiber-based polarization controller (PC). After filtering by a polarizer oriented at 45°, the photon is sent into a Mach–Zehnder interferometer (MZI) with two arms of equal lengths. In the MZI, a set of half-wave-plates (HWP), quarter-wave-plates (QWP), and PBSs are applied at 3 different times (denoted as t_1, t_2 and t_3 in the figure) to perform the projective measurements and polarization recovery operations for the τGHZ test. All of the wave-plates are mounted on motorized precision rotation mounts that are automatically controlled by a computer. A prism, positioned on a one-axis motorized translation stage, is used to precisely adjust the length of one arm so that the two spatial modes in the MZI coherently interfere with each other at the PBS7 before readout by detector D2 with a detection efficiency of 50% at 808 nm. We register the two-fold coincidence counts between D1 and D2 with a 5 ns window through a home-made Field-Programmable Gate Array (FPGA) board. The GHZ test is repeated with 32 trials, each with different angles of the wave-plates (see the Appendix). To guarantee that the phase of the MZI is stable during the measurement, we monitor the count rate C_{ref} with a fixed wave-plate setting before and after each trial.

Let PBS$(\alpha, \overline{\alpha})$ denote that the PBS transmits the photon in the $|\alpha\rangle$ polarization and reflects the orthogonal component $|\overline{\alpha}\rangle$, while WP$(\beta, \gamma)$ denote that the WP is set up so that the incoming photon in the $|\beta\rangle$ polarization is transformed into the $|\gamma\rangle$ polarization. Then for a given trial, the settings have the form

$$\begin{aligned}\{&\text{PBS1}(x_i, \overline{x}_i),\ \text{WP3}(x_i, \text{H}),\ \text{PBS2}(x_i, \overline{x}_i),\ \text{WP4}(x_i, \text{V}),\\ &\text{PBS3}(x_j, \overline{x}_j),\ \text{WP5}(x_j, \text{H}),\ \text{PBS4}(x_j, \overline{x}_j),\ \text{WP6}(x_j, \text{V}),\\ &\text{PBS5}(x_k, \overline{x}_k),\ \text{WP7}(x_k, \text{H}),\ \text{PBS6}(x_k, \overline{x}_k),\ \text{WP8}(x_k, \text{V})\}\end{aligned}$$

with fixed values of $i, j, k = 1, 2, 3$.

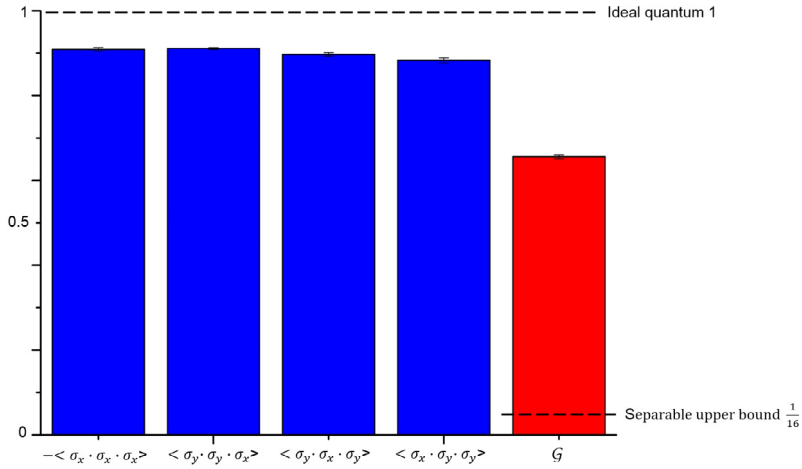

Fig. 2. We show the measurement results (0.909(4), 0.911(2), 0.897(4), 0.883(6)) corresponding to four different bases and the measured functional $\mathcal{G} = 0.656(5)$ which is clearly larger than 1/16. The error bars account for the statistical error associated with the photon counting by assuming a Poissonian distribution of the photon counts. Systematic errors are discussed in the Appendix.

We define

$$C_{i,j,k} := \frac{\text{Counts}_{i,j,k}(\text{D2})}{\text{Counts}(\text{total})}$$

where Counts(total) denotes the overall number of photons sent into the MZI, which is a constant for different trials in our experiment. By collecting data from all of the trials we can evaluate

$$\langle \sigma_x \odot \sigma_x \odot \sigma_x \rangle = \frac{C_{1,1,1} - C_{1,1,2} - C_{1,2,1} + C_{1,2,2} - C_{2,1,1} + C_{2,1,2} + C_{2,2,1} - C_{2,2,2}}{C_{1,1,1} + C_{1,1,2} + C_{1,2,1} + C_{1,2,2} + C_{2,1,1} + C_{2,1,2} + C_{2,2,1} + C_{2,2,2}} \tag{18}$$

$$\langle \sigma_y \odot \sigma_y \odot \sigma_x \rangle = \frac{C_{3,3,1} - C_{3,3,2} - C_{3,4,1} + C_{3,4,2} - C_{4,3,1} + C_{4,3,2} + C_{4,4,1} - C_{4,4,2}}{C_{3,3,1} + C_{3,3,2} + C_{3,4,1} + C_{3,4,2} + C_{4,3,1} + C_{4,3,2} + C_{4,4,1} + C_{4,4,2}} \tag{19}$$

$$\langle \sigma_y \odot \sigma_x \odot \sigma_y \rangle = \frac{C_{3,1,3} - C_{3,1,4} - C_{3,2,3} + C_{3,2,4} - C_{4,1,3} + C_{4,1,4} + C_{4,2,3} - C_{4,2,4}}{C_{3,1,3} + C_{3,1,4} + C_{3,2,3} + C_{3,2,4} + C_{4,1,3} + C_{4,1,4} + C_{4,2,3} + C_{4,2,4}} \tag{20}$$

$$\langle \sigma_x \odot \sigma_y \odot \sigma_y \rangle = \frac{C_{1,3,3} - C_{1,3,4} - C_{1,4,3} + C_{1,4,4} - C_{2,3,3} + C_{2,3,4} + C_{2,4,3} - C_{2,4,4}}{C_{1,3,3} + C_{1,3,4} + C_{1,4,3} + C_{1,4,4} + C_{2,3,3} + C_{2,3,4} + C_{2,4,3} + C_{2,4,4}} \tag{21}$$

and finally compute

$$\mathcal{G}[|\Psi\rangle] = -\langle \sigma_x \odot \sigma_x \odot \sigma_x \rangle \langle \sigma_y \odot \sigma_y \odot \sigma_x \rangle \langle \sigma_y \odot \sigma_x \odot \sigma_y \rangle \langle \sigma_x \odot \sigma_y \odot \sigma_y \rangle$$

by taking the product.

The four measured correlations are shown in Fig. 2. The computed value of $\mathcal{G}$ is 0.656 ± 0.005, where the error bars take into account the statistics of detector photocounting. To calculate the error bars, we apply a Monte Carlo simulation by assuming a Poissonian distribution of the photon counts. The deviation between the measured $\mathcal{G} = 0.656 \pm 0.005$ and ideal value 1 mainly comes from the imperfection of the M–Z interferometer and multi-photon-pair events from our SPDC source (see Appendix for the error analysis).

Similar to most optical experiments, due to photon loss and low detection efficiency of the single photon detector (≈50% at 808 nm), we have to discard the events when neither APD2 nor APD3 fire.

This opens up a detection-efficiency loophole, and we need to assume that the detected events can fairly represent a statistical sample of all the emitted photons (i.e., a fair sampling assumption).

5. Conclusion

We have performed an experiment to create and validate an entangled history state for a single photon. The experiment allows us to superpose radically different versions of the system's history, and to probe its entangled structure. The experimental results violate inequalities implied by separability by a large margin. These results support that the best description of the history of a quantum system can contain multiple interwoven timelines or sequences of events. The experiment realizes the possibility of more exotic probes of temporal correlations in controlled quantum systems. More interesting temporal correlations arise for entangled histories of more than one particle (in our case, a single photon) [2], which have not yet been explored experimentally.

It may seem startling that a version of the GHZ phenomenon, which in many ways epitomizes the peculiar characteristics of quantum theory, can be reproduced using, in essence, classical optics. Other examples of quantum phenomena being captured by a classical description have also been of recent interest [48,49]. On the other hand, we may recall that Dirac's magisterial text on quantum theory begins with a long discussion of experiments with polarized light [50]. Indeed, the wave theory of light already supports the principle of superposition, the calculation of intensities through squares of amplitudes, and interference phenomena — i.e., the central aspects of quantum-mechanical wave functions. In our context, the central innovation of quantum theory is not to change the rules of wave theory, but to allow an alternative (particle) interpretation of its results. By following out that particle interpretation fully we discover that it brings in new ideas, such as the temporal entanglement of histories.

Acknowledgments

JC and FW are grateful to Sandu Popescu and Michael Walter for discussions and valuable insights. We also thank the reviewers for thoughtful feedback. JC is supported by the Fannie and John Hertz Foundation and the Stanford Graduate Fellowship program. FW's work is supported by the U.S. Department of Energy under Grant Contract Number DE-SC0012567. LMD acknowledges support from the IARPA MUSIQC program, the AFOSR and the ARO MURI program. ZQY is supported by the National Natural Science Foundation of China Grant 61435007 and 11574176.

Appendix

A.1. A classical calculation

Here we analyze a class of classical systems which have qualitative similarities to the τGHZ test. The assumptions for our calculations are as follows. Suppose that we have three observers A, B, C who measure the value of σ_x or σ_y at three different times t_1, t_2 and t_3. The measurement basis (the x-basis or the y-basis) is chosen randomly at each time. Communication among A, B and C is forbidden for $t_1 \leq t \leq t_3$. Then at a later time t_4 (after time t_3), A, B and C exchange information on their choice of basis and measurement results. When their basis choices correspond to the $\mathcal{G}$ functional choices (e.g. σ_x for t_1, σ_x for t_2, and σ_x for t_3), and only then, the measured results are recorded.

One can imagine more complicated classical models in which A can source information to B and B can source information to C, even though we know that the underlying quantum mechanical description of our system does not entail A, B and C secretly collaborating, since we correct the state of the photon after each intermediate measurement to what it was before the measurement. We are not interested in ruling out more complicated classical possibilities, or precluding the existence of macrorealistic theories. Rather, we are content with the correctness of quantum mechanics in the present circumstances, and simply wish to gain intuition from a classical model.

In our classical model, the observable values at the three different times are allowed to be correlated. Thus we introduce a master joint total distribution $\chi(Q_x^1, Q_y^1, Q_x^2, Q_y^2, Q_x^3, Q_y^3)$, and calculate

$$\mathcal{G}[\chi] = -(Q_x^1 Q_x^2 Q_x^3)_\chi (Q_x^1 Q_y^2 Q_y^3)_\chi (Q_y^1 Q_x^2 Q_y^3)_\chi (Q_y^1 Q_y^2 Q_x^3)_\chi \tag{22}$$

in an evident notation.

There are eight possible assignments of the products of these variables consistent with the classical constraint that the product of their products is unity. Let us define their probabilities with respect to the distribution χ as follows:

$$\begin{aligned}
&\text{Prob}(Q_x^1 Q_x^2 Q_x^3 = +1, Q_x^1 Q_y^2 Q_y^3 = +1, Q_y^1 Q_x^2 Q_y^3 = +1, Q_y^1 Q_y^2 Q_x^3 = +1) \equiv p_1\\
&\text{Prob}(Q_x^1 Q_x^2 Q_x^3 = +1, Q_x^1 Q_y^2 Q_y^3 = -1, Q_y^1 Q_x^2 Q_y^3 = -1, Q_y^1 Q_y^2 Q_x^3 = +1) \equiv p_2\\
&\text{Prob}(Q_x^1 Q_x^2 Q_x^3 = +1, Q_x^1 Q_y^2 Q_y^3 = -1, Q_y^1 Q_x^2 Q_y^3 = +1, Q_y^1 Q_y^2 Q_x^3 = -1) \equiv p_3\\
&\text{Prob}(Q_x^1 Q_x^2 Q_x^3 = +1, Q_x^1 Q_y^2 Q_y^3 = +1, Q_y^1 Q_x^2 Q_y^3 = -1, Q_y^1 Q_y^2 Q_x^3 = -1) \equiv p_4\\
&\text{Prob}(Q_x^1 Q_x^2 Q_x^3 = -1, Q_x^1 Q_y^2 Q_y^3 = -1, Q_y^1 Q_x^2 Q_y^3 = -1, Q_y^1 Q_y^2 Q_x^3 = -1) \equiv p_5\\
&\text{Prob}(Q_x^1 Q_x^2 Q_x^3 = -1, Q_x^1 Q_y^2 Q_y^3 = -1, Q_y^1 Q_x^2 Q_y^3 = +1, Q_y^1 Q_y^2 Q_x^3 = +1) \equiv p_6\\
&\text{Prob}(Q_x^1 Q_x^2 Q_x^3 = -1, Q_x^1 Q_y^2 Q_y^3 = +1, Q_y^1 Q_x^2 Q_y^3 = -1, Q_y^1 Q_y^2 Q_x^3 = +1) \equiv p_7\\
&\text{Prob}(Q_x^1 Q_x^2 Q_x^3 = -1, Q_x^1 Q_y^2 Q_y^3 = +1, Q_y^1 Q_x^2 Q_y^3 = +1, Q_y^1 Q_y^2 Q_x^3 = -1) \equiv p_8
\end{aligned} \tag{23}$$

Then for the GHZ functional we have

$$\begin{aligned}
\mathcal{G}[\chi] = &-(p_1 + p_2 + p_3 + p_4 - p_5 - p_6 - p_7 - p_8)(p_1 + p_2 - p_3 - p_4 - p_5 + p_6 + p_7 - p_8)\\
&(p_1 - p_2 + p_3 - p_4 - p_5 + p_6 - p_7 + p_8)(p_1 - p_2 - p_3 + p_4 - p_5 - p_6 + p_7 + p_8)
\end{aligned} \tag{24}$$

Maximizing this over probability distributions, we find that it is bounded below by

$$\mathcal{G}[\chi] \leq \frac{1}{16} \tag{25}$$

The maximum is assumed at $(p_1, p_2, p_3, p_4, p_5, p_6, p_7, p_8) = (\frac{1}{4}, \frac{1}{4}, \frac{1}{4}, 0, 0, \frac{1}{4}, 0, 0)$ and at several other points. It is intriguing that Eq. (25) is the same bound satisfied by history states lacking tripartite entanglement.

A.2. Partially separable history state

We consider a two-time entangled history with an attached separable history state. Such a state has the form $|\psi) \odot \begin{bmatrix} \cos^2(\theta) & \cos(\theta)\sin(\theta)e^{-i\phi} \\ \cos(\theta)\sin(\theta)e^{i\phi} & \sin^2(\theta) \end{bmatrix}$, where $|\psi)$ is an arbitrary two-time entangled history states. As mentioned in the paper, other history states with two-time entanglement take the same form, up to permutations of the tensor product components. It suffices to consider a single ordering since the $\mathcal{G}$ functional is not sensitive to such permutations. The above history state gives

$$\mathcal{G} = -\frac{1}{4}\sin^4(2\theta)\sin^2(2\phi)\langle\sigma_X \odot \sigma_X\rangle\langle\sigma_X \odot \sigma_Y\rangle\langle\sigma_Y \odot \sigma_X\rangle\langle\sigma_Y \odot \sigma_Y\rangle \tag{26}$$

The term $\frac{1}{4}(\sigma_X \odot \sigma_X)(\sigma_X \odot \sigma_Y)(\sigma_Y \odot \sigma_X)(\sigma_Y \odot \sigma_Y)$ can be written by expanding in a basis of temporal Bell states. Let us write

$$|\psi) = a|\phi^+) + b|\phi^-) + c|\psi^+) + d|\psi^-) \tag{27}$$

where the basis vectors are the four temporal Bell states, and $|a|^2 + |b|^2 + |c|^2 + |d|^2 = 1$. For the two-time entangled history state $|\psi)$, we get

$$\mathcal{G}[|\psi)] = -((|c|^2 - |d|^2)^2 - (|a|^2 - |b|^2)^2)((a^*b - b^*a)^2 - (c^*d - d^*c)^2) \tag{28}$$

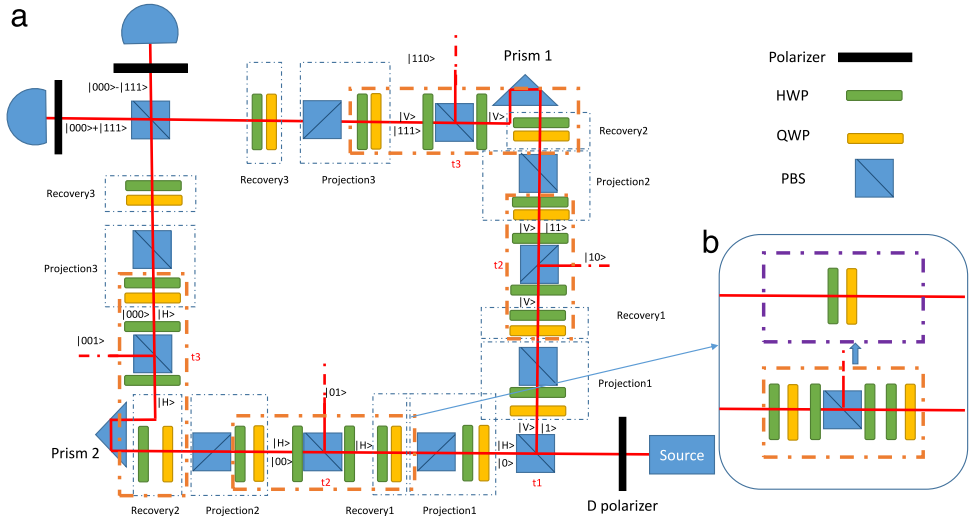

Fig. 3. Detailed experimental design of temporal GHZ test. (For interpretation of the references to color in this figure legend, the reader is referred to the web version of this article.)

By adding extra phase parameters ϕ_{ab} and ϕ_{cd} we can write Eq. (26) as

$$\mathcal{G} = -\sin^4(2\theta)\sin^2(2\phi)((|c|^2 - |d|^2)^2 - (|a|^2 - |b|^2)^2)((|a||b|\sin(\phi_{ab}))^2 - (|c||d|\sin(\phi_{cd}))^2) \tag{29}$$

Optimizing over $|a|$, $|b|$, $|c|$, $|d|$, ϕ_{ab} and ϕ_{cd} subject to the appropriate constraints, we find that for the class of history states under consideration, the maximum value for $\mathcal{G}$ is exactly $1/16$.

We note that this analysis only tells us that the partially separable history state given above does not have the same kind of temporal entanglement as the temporal GHZ history state. To show that the partially separable state does not have any tripartite entanglement in time, we would instead have to use a temporal analogue of the Svetlichny inequality [51,52].

A.3. Experimental design

In our experiment (Fig. 3), we prepare a heralded single photonic qubit through a spontaneous parametric down-conversion process (SPDC). We encode our spin-1/2 particle into the polarization degree of freedom of our single photon, and prepare the qubit state to $|D\rangle = \frac{1}{\sqrt{2}}(|H\rangle + |V\rangle)$ with a polarizer. At time t_1, we apply a polarizing beamsplitter (PBS), which transmits horizontal light ($|H\rangle$) and reflects vertical light ($|V\rangle$), to perform the controlled-NOT gate. The first auxiliary qubit is encoded into the two different out-ports of the first PBS, where transmission corresponds to $|0\rangle$ and reflection corresponds to $|1\rangle$. After the first PBS, our two-qubit state is $\frac{1}{\sqrt{2}}(|H\rangle|0\rangle + |V\rangle|1\rangle)$. In order to perform the projective measurement on our spin-1/2 particle, we apply a HWP, a QWP followed by a PBS on each arm (labeled as Projection 1). After the projective measurement, we apply another set of wave-plates on each arm to recover the spin state back to its initial state (labeled as recovery 1). After the recovery, we apply a HWP, a PBS and another HWP at time t_2 on each arm to perform the second CNOT gate, with the second auxiliary qubit encoded in the two out-ports of the PBS (on the upper arm, the transmission port is encoded as $|1\rangle$, while at the lower arm, the transmission port is encoded as $|0\rangle$). Note that at time t_2, the HWP before the PBS is used to rotate the polarization so that the photon fully transmits, and the HWP after the PBS is used to rotate the photonic state back to its initial polarization. Then at t_2 we get the state $\frac{1}{\sqrt{2}}(|H\rangle|0\rangle|0\rangle + |V\rangle|1\rangle|1\rangle)$. We follow the same strategy

Table 1
Angles of wave-plates.

	QWP1	HWP1	QWP2	HWP2	QWP3	HWP3	QWP4	HWP4	QWP5	HWP5	QWP6	HWP6	QWP7	HWP7	QWP8	HWP8
Ref	0	45	0	0	0	0	0	45	0	0	0	0	0	0	0	0
Trial1.1	135	67.5	90	112.5	90	112.5	90	45	135	67.5	90	67.5	90	67.5	90	90
Trial1.2	45	112.5	90	112.5	90	112.5	90	45	45	112.5	90	67.5	90	67.5	90	90
Trial1.3	135	67.5	90	67.5	90	112.5	90	45	135	67.5	90	22.5	90	67.5	90	90
Trial1.4	45	112.5	90	67.5	90	112.5	90	45	45	112.5	90	22.5	90	67.5	90	90
Trial1.5	135	67.5	90	112.5	90	67.5	90	45	135	67.5	90	67.5	90	22.5	90	90
Trial1.6	45	112.5	90	112.5	90	67.5	90	45	45	112.5	90	67.5	90	22.5	90	90
Trial1.7	135	67.5	90	67.5	90	67.5	90	45	135	67.5	90	22.5	90	22.5	90	90
Trial1.8	45	112.5	90	67.5	90	67.5	90	45	45	112.5	90	22.5	90	22.5	90	90
Trial2.1	90	67.5	45	22.5	90	112.5	90	45	90	67.5	315	22.5	90	67.5	90	90
Trial2.2	90	112.5	45	22.5	90	112.5	90	45	90	112.5	315	22.5	90	67.5	90	90
Trial2.3	90	67.5	315	22.5	90	112.5	90	45	90	67.5	45	22.5	90	67.5	90	90
Trial2.4	90	112.5	315	22.5	90	112.5	90	45	90	112.5	45	22.5	90	67.5	90	90
Trial2.5	90	67.5	45	22.5	90	67.5	90	45	90	67.5	315	22.5	90	22.5	90	90
Trial2.6	90	112.5	45	22.5	90	67.5	90	45	90	112.5	315	22.5	90	22.5	90	90
Trial2.7	90	67.5	315	22.5	90	67.5	90	45	90	67.5	45	22.5	90	22.5	90	90
Trial2.8	90	112.5	315	22.5	90	67.5	90	45	90	112.5	45	22.5	90	22.5	90	90
Trial3.1	90	67.5	90	112.5	45	22.5	90	45	90	67.5	90	67.5	315	22.5	90	90
Trial3.2	90	112.5	90	112.5	45	22.5	90	45	90	112.5	90	67.5	315	22.5	90	90
Trial3.3	90	67.5	90	67.5	45	22.5	90	45	90	67.5	90	22.5	315	22.5	90	90
Trial3.4	90	112.5	90	67.5	45	22.5	90	45	90	112.5	90	22.5	315	22.5	90	90
Trial3.5	90	67.5	90	112.5	315	22.5	90	45	90	67.5	90	67.5	45	22.5	90	90
Trial3.6	90	112.5	90	112.5	315	22.5	90	45	90	112.5	90	67.5	45	22.5	90	90
Trial3.7	90	67.5	90	67.5	315	22.5	90	45	90	67.5	90	112.5	45	22.5	90	90
Trial3.8	90	112.5	90	67.5	315	22.5	90	45	90	112.5	90	112.5	45	22.5	90	90
Trial4.1	45	67.5	45	22.5	45	22.5	90	45	45	67.5	315	22.5	315	22.5	90	90
Trial4.2	135	112.5	45	22.5	45	22.5	90	45	135	112.5	315	22.5	315	22.5	90	90
Trial4.3	45	67.5	315	22.5	45	22.5	90	45	45	67.5	45	22.5	315	22.5	90	90
Trial4.4	135	112.5	315	22.5	45	22.5	90	45	135	112.5	45	22.5	315	22.5	90	90
Trial4.5	45	67.5	45	22.5	315	22.5	90	45	45	67.5	315	22.5	45	22.5	90	90
Trial4.6	135	112.5	45	22.5	315	22.5	90	45	135	112.5	315	22.5	45	22.5	90	90
Trial4.7	45	67.5	315	22.5	315	22.5	90	45	45	67.5	45	22.5	45	22.5	90	90
Trial4.8	135	112.5	315	22.5	315	22.5	90	45	135	112.5	45	22.5	45	22.5	90	90

to perform the second projective measurement on our spin-1/2 qubit, the third CNOT gate at time t_3, and finally the third projective measurement followed by the third recovery operation. After that, our spin-1/2 qubit and three auxiliary qubits are in the final state $\frac{1}{\sqrt{2}}(|H\rangle|0\rangle|0\rangle|0\rangle + |V\rangle|1\rangle|1\rangle|1\rangle)$. To project the three auxiliary qubits in the GHZ basis $\frac{1}{\sqrt{2}}(|000\rangle \pm |111\rangle)$, we interfere the two arms at the final PBS, and use a polarizer and a fiber-based single photon detector at each out-port to detect the state.

In the real experiment, we simplify the optics in each orange dashed box to a HWP and QWP (the purple dashed box in the inset of Fig. 3). This simplification does not change any of our measurement results, since we let the signal fully transmit on the PBS at time t_2 and t_3. Such a simplification also improves the stability of our M–Z interferometer since the overall size is smaller.

A.4. Error analysis

In our experiment, the extinction ratio of our PBS is greater than 100:1. We use a motorized precision rotation mount to control the angle of the wave-plates within 0.1% accuracy. The axes of the wave-plates and polarizers have been carefully calibrated within 1°. We minimize the imbalance of the M–Z interferometer such that the photon collection efficiency from the two arms is within 1%. The deviation between the measured $\mathcal{G} = 0.656 \pm 0.005$ and ideal value 1 mainly comes from the imperfection of the M–Z interferometer. In the experiment, we observe a 94% interference contrast, where the error is caused by imperfect temporal and spatial overlap between the two arms, and the phase fluctuations (mainly due to temperature drifting and air current) during the data accumulation procedure. In addition, since photon pair generation from the SPDC is a probabilistic process, we inevitably have a small probability (2%) to prepare multiple heralded photons at the same time. Such multi-photon events also take partial responsibility for the deviation from our expected answer.

A.5. Wave-plates parameters for experiment

See Table 1.

References

[1] Robert Griffiths, Consistent Quantum Theory, Cambridge UP, Cambridge, 2002. Print.
[2] Jordan Cotler, Frank Wilczek, Entangled histories. arXiv:1502.02480, 2015.
[3] Jordan Cotler, Frank Wilczek, Bell test for histories. arXiv:1503.06458, 2015.
[4] Jordan Cotler, Frank Wilczek, Phys. Scr. 2016 (T168) (2016) 014004.
[5] A. Einstein, B. Podolsky, N. Rosen, Phys. Rev. 47 (1935) 777.
[6] J.S. Bell, Physics 1 (1964) 195.
[7] J.S. Bell, Epistemol. Lett. 9 (11) (1976).
[8] S.J. Freedman, J.F. Clauser, Phys. Rev. Lett. 28 (1972) 938.
[9] A. Aspect, J. Dalibard, G. Roger, Phys. Rev. Lett. 49 (1804) (1982).
[10] B. Hensen, et al., Nature 526 (2015) 682.
[11] D. Greenberger, M. Horne, A. Zeilinger, Bell's Theorem, Quantum Theory, and Conceptions of the Universe, Kluwer, Dordrecht, 1989, pp. 69–72.
[12] D. Mermin, Am. J. Phys. 58 (8) (1990) 731–734.
[13] S. Coleman, Quantum Mechanics in Your Face, lecture at New England sectional meeting of APS, 1994.
[14] Jian-Wei Pan, et al., Nature 403 (2000) 515.
[15] Anthony J. Leggett, Anupam Garg, Phys. Rev. Lett. 54 (9) (1985) 857.
[16] Anthony J. Leggett, Found. Phys. 18 (9) (1988) 939–952.
[17] Anthony J. Leggett, Rep. Progr. Phys. 71 (2) (2008) 022001.
[18] J.P. Paz, G. Mahler, Phys. Rev. Lett. 71 (1993) 3235.
[19] Caslav Brukner, et al., Quantum entanglement in time. arXivquant-ph/0402127, 2004.
[20] Tobias Fritz, New J. Phys. 12 (8) (2010) 083055.
[21] Neill Lambert, et al., Phys. Rev. Lett. 105 (17) (2010) 176801.
[22] G. Waldherr, et al., Phys. Rev. Lett. 107 (2011) 090401.
[23] Neill Lambert, Robert Johansson, Franco Nori, Phys. Rev. B 84 (24) (2011) 245421.
[24] Clive Emary, Neill Lambert, Franco Nori, Phys. Rev. B 86 (23) (2012) 235447.
[25] Clive Emary, Neill Lambert, Franco Nori, Rep. Progr. Phys. 77 (1) (2014) 016001.
[26] Neill Lambert, et al., Phys. Rev. A 94 (1) (2016) 012105.

[27] Shin-Liang Chen, et al., Phys. Rev. Lett. 116 (2) (2016) 020503.
[28] Karol Bartkiewicz, et al., Sci. Rep. 6 (2016).
[29] Karol Bartkiewicz, et al., Phys. Rev. A 93 (6) (2016) 062345.
[30] Huan-Yu Ku, et al., Phys. Rev. A 94 (6) (2016) 062126.
[31] Roland Omnés, Phys. Lett. A 125 (4) (1987) 169–172. Web.
[32] Roland Omnés, The Interpretation of Quantum Mechanics, Princeton UP, Princeton, NJ, 1994. Print.
[33] Murray Gell-Mann, James B. Hartle, Complexity, Entropy and the Physics of Information (1990) 321–343.
[34] Murray Gell-Man, J. Hartle, Proceedings of the 25th International Conference on High Energy Physics, Singapore, 1990.
[35] James B. Hartle, Quantum Cosmology and Baby Universes, Vol. 1, 1991.
[36] C.J. Isham, J. Math. Phys. 35 (5) (1994) 2157.
[37] C.J. Isham, N. Linden, J. Math. Phys. 35 (10) (1994) 5452.
[38] C.J. Isham, N. Linden, J. Math. Phys. 36 (10) (1995) 5392.
[39] C.J. Isham, Internat. J. Theoret. Phys. 36 (4) (1997) 785–814. Print.
[40] Y. Aharonov, S. Popescu, J. Tollaksen, L. Vaidman, Phys. Rev. A 79 (2009) 052110.
[41] George C. Knee, et al., Nat. Commun. 3 (2012) 606.
[42] Carsten Robens, et al., Phys. Rev. X 5 (1) (2015) 011003.
[43] Hemant Katiyar, Experimental violation of the Leggett-Garg inequality in a 3-level system. arXiv:1606.07151, 2016.
[44] J.J. Halliwell, Phys. Rev. A 94 (5) (2016) 052131.
[45] Jordan Cotler, Frank Wilczek, Entanglement enabled intensity interferometry. arXiv:1502.02477, 2015.
[46] A. Danan, D. Farfurnik, S. Bar-Ad, L. Vaidman, Phys. Rev. Lett. 111 (2013) 240402.
[47] E. Megidish, et al., Phys. Rev. Lett. 110 (2013) 210403.
[48] Sacha Kocsis, et al., Science 332 (6034) (2011) 1170–1173.
[49] Konstantin Y. Bliokh, et al., New J. Phys. 15 (7) (2013) 073022.
[50] P.A.M. Dirac, The Principles of Quantum Mechanics, Vol. 27, Oxford University Press, 1981.
[51] George Svetlichny, Phys. Rev. D 35 (10) (1987) 3066.
[52] Peter Mitchell, Sandu Popescu, David Roberts, Phys. Rev. A 70 (6) (2004) 060101.